www.czasopisma.pan.pl PAN www.journals.pan.pl
Opto-Electronics Review 26 (2018) 1–10

Contents lists available at ScienceDirect

Opto-Electronics Review

journal homepage: http://www.journals.elsevier.com/opto-electronics review

Enhancement in NBE emission and optical band gap by Al doping in nanocrystalline ZnO thin films

N. Kumar, A. Srivastava *

Department of Physics, University of Lucknow, Lucknow, 226007, India

ARTICLE INFO

Article history:
Received 12 April 2017
Received in revised form 2 October 2017
Accepted 5 November 2017
Available online 5 December 2017

Keywords:
Al doped ZnO
Spray pyrolysis
Band-gap
Enhanced UV-emission
Suppression of defect-emission

ABSTRACT

Transparent Al doped ZnO nanocrystalline films with a crystallite size less than 19 nm are obtained by spray pyrolysis. Band gap increases monotonically from 3.16 to 3.31 eV with increasing aluminum dopant up to 1.56 at.% facilitating increasing width of a transmission window in addition to the band gap tuning of 4.74% which compares favorably well with literature. UV emission with continuously increasing intensity is obtained which reflects on the good crystalline quality of the films. Also the defect emissions are suppressed remarkably as the dopant Al concentration increases in ZnO. The band gap tuning by quite small increment in dopant amount makes the present films, much attractive for the fabrication of light emitting devices with a much sought-for benefit of large area fabrication. FESEM shows the surface is granular with grain size lying in the range of 20–35 nm and EDX confirms the presence of Al in the doped samples

1. Introduction

Band-gap engineering of ZnO is an area of continuous interest for developing transparent photonic devices, transparent electronics and transparent conducting electrodes [1–3]. ZnO also caters surface acoustic wave devices [4], solar cells [5], flat panel display [6] etc. besideothers. Transparent conducting layer of Al-doped ZnO nanowire thin film has been used in dye-sensitized solar cells [7]. ZnO based nanowires also show good performance in applications such as energy harvesting, flexible electronics etc.[8]. Sensing of gases using hybrid ZnO-Bi_2O_3 and ZnO-Zn_2SnO_4 tetrapod networks has also been reported [9]. Broadband photo-absorption has been obtained by stretchable 3D hybrid architectures based on aerographite decorated by nano- and micro- scale tetrapods of ZnO [10].

A wide direct band gap of about 3.37 eV facilitates optical transparency to ZnO over the entire visible region. Additionally, its large exciton binding energy of 60 meV at room temperature leads to photoluminescence properties [11]. Generally, ZnO exhibits a blue-green emission at room temperature regardless of the fabrication conditions and techniques. The green photoluminescence from ZnO structures is thought to be due to surface defects viz. singly ionized oxygen vacancies, Zn interstitials, Zn vacancies etc.[12].Various nanostructures can be grown in zinc oxide. ZnO tetrapods and their networks fabricated using flame transport synthesis (FTS) exhibit promising photocatalytic and photoswitching behaviours. Network of these structures have rewarding features such as high-temperature stability, electrical conductivity, tunable Young's modulus etc. which open up numerous areas not only in basic research but also for industrial applications. In addition to ZnO, nano- and microstructures of SnO_2 [13] and several other metal oxides can be synthesized by the FTS [14]. A sample having direct integration of ZnO nano- and micro- needles using FTS shows NBE emission located around ~380 nm and a broad green luminescence due to deep level defects [15]. Isoelectronic dopants such as Ca, Mg, Sr etc. have been added to ZnO to tune its band gap whereas Group III metal dopants viz. Al, In, Ga have been suitably added to increase the electrical conductivity and transparency of ZnO films [16–18]. Out of these dopants, aluminum has proved to be effective in obtaining high quality samples with increased transparency to visible light and emission in UV/blue region [19]. Additionally, due to Burstein-Moss effect (BM), band gap also gets altered. With naturally occurring n-type conductivity and optical transparency, zinc oxide is emerging as a potential alternative to ITO for thin film transparent electrode applications. Doped ZnO films which are reported to be comparatively more stable, both thermally [20–24] and electrically, can be obtained using various physical deposition methods – PLD, sputtering, thermal evaporation, magnetron sputtering [25] etc. – where maintenance of vacuum is essential; as well

* Corresponding author.
E-mail addresses: nishant1986lu@gmail.com (N. Kumar), asrivastava.lu@gmail.com (A. Srivastava).

https://doi.org/10.1016/j.opelre.2017.11.001
1230-3402/

as chemical vapour deposition and wet chemical routes [26–31]. Here in the present work Al doped ZnO films are obtained by spray pyrolysis -a wet chemical route capable of large area deposition with no requirement of vacuum. The effect of doping on optical properties, i.e. transmission, band gap and photoluminescence is the main focus of this paper besides study of structure and surface of the film. The optical properties of ZnO based films largely depend on the surface morphology [32].

2. Experimental

The precursor solution of undoped ZnO is prepared by dissolving 2 gm of zinc acetate dihydrate (Merck India, 99.00%) in 45 ml ethanol (Hayman, UK, 99.723%) to obtain a molarity of 0.2 M. Ten drops of diethanolamine (Merck India 98.9%) were also used at the time of mixing as described in Ref. [20]. For 1, 2 ad 3 at.% Al doping, 0.0339, 0.0674 and 0.1004 gm of $Al(NO_3)_3{\cdot}9H_2O$ is dissolved in 0.45, 0.90 and 1.33 ml of ethanol, respectively; separate solutions of 1.966, 1.932 and 1.899 gm of zinc acetate dihydrate are prepared in 44.8, 44.0 and 43.2 ml of ethanol, respectively. Next, both the precursor solutions are mixed together to obtain precursor solutions for 1, 2, and 3 at% Al doped ZnO which are then aged for five days before spraying them on separate substrates using the experimental set-up described in Ref. [26]. The flow rate was kept at 1.0 ml per min with nozzle-substrate distance of 20 cm and substrate temperature of 400 °C. Annealing, essential for obtaining good quality stabilized films, was carried for 4 h at 450 °C. The entire process is shown in flowchart, Fig. 1. The four sample films deposited using precursors with 0, 1, 2 and 3 at.% Al doping in ZnO are named as AZ0, AZ1, AZ2 and AZ3, respectively.

The crystal phase and crystallinity of the samples have been investigated using X-Ray diffractometer (Model – PANalytical X'Pert PRO X-ray diffractometer) for 2θ values ranging from 25 to 80° using CuKα radiation (λ = 1.54184 Å). The energy dispersive analysis (EDX) and surface morphology is obtained using FESEM (Model- ZEISS). Transmission spectra and photoluminescence (PL) spectra have been recorded using UV–vis spectrophotometer (Model- V670, Jasco) and fluorescence spectrometer with a 20 kW Xe discharge lamp (Model- LS-55, Perkin Elmer), respectively. During PL measurement, the experimental settings such as excitation wavelength (325 nm), excitation and emission slit width (15 nm) and step size (0.5 nm), were kept the same for all the samples. All the measurements were performed at room temperature.

3. Results and discussion

3.1. X – ray diffraction

The XRD patterns (Fig. 2) correspond to the hexagonal wurtzite structure of ZnO showing noticeable orientation along (100), (002) and (101) plane [33] with (002) plane as the most preferred one. Also, any impurity phase does not appear in the doped films. The peak along c-axis, i.e. (002) plane occurs at 2θ=34.424°, 34.384°, 34.284° and 34.584° for samples AZ0, AZ1, AZ2 and AZ3, respectively. The diffraction peak shifts to a lower value of 2θ for AZ1 and AZ2. For sample AZ3 the angle of diffraction increases becoming more than that for AZ0. The orientation parameter $\gamma_{(hkl)}$ [29,34] varies from 0.141 to 0.286 with the maximum value along (002) plane (Table 1). For all the samples crystallite size, as calculated from Debye-Scherrer (DS) formula, varies from 9 to 19 nm [35,36]. Williamson and Hall plot [37] shown in Fig. 3 has been obtained using full width at half maximum (FWHM, β) of the XRD peaks and the corresponding diffraction angles to study size and strain induced line broadening. The trend line equations of the plots in Fig. 3 are found to be $y = -0.0585x + 0.0272$, $y = -0.0233x + 0.0148$, $y = -0.0063x + 0.0100$ and $y = 0.1654x - 0.0367$ for samples AZ0 to AZ3, respectively. These equations when compared to $\beta\cos\theta = C\lambda/t_{WH} + 2\varepsilon\sin\theta$ give the strain ε and crystallite size t_{WH} in the films (Table 1). C, the correction factor is taken as 1. Value of the strain is found to vary from -3.15×10^{-4} to 8.270×10^{-2}. Negative and positive signs indicate the compressive and tensile strains respectively. Strain in sample AZ2 is less by two orders as compared to those in other samples and this is also reflected by the approximately same particle size

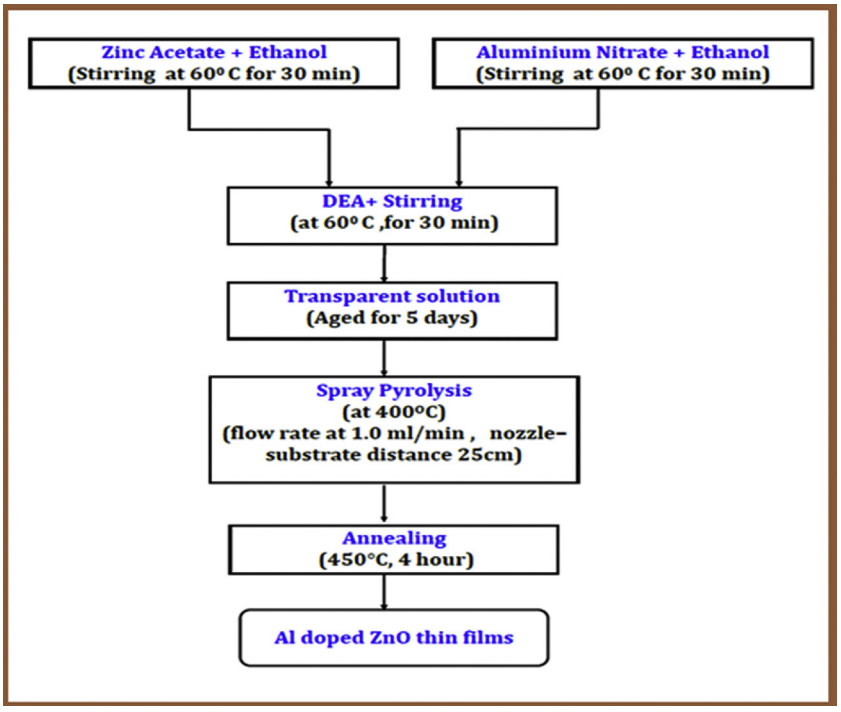

Fig. 1. Process for obtaining the precursor and the films.

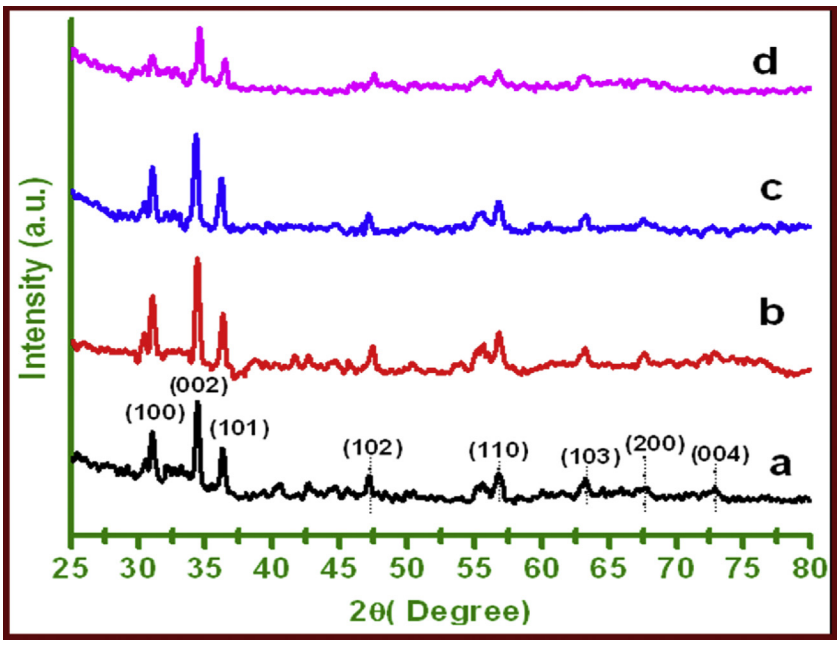

Fig. 2. XRD spectra for undoped and Al doped thin films. Curves a–d correspond to samples AZ0, AZ1, AZ2 and AZ3, respectively.

Table 1
Crystallite size determined by DS formula and WH plot, strain and orientation parameter along different planes for undoped and Al doped films.

Samples	t_{DS} (nm)			t_{WH} (nm)	Strain ε	Orientation Parameter γ(hkl)		
	(100)	(002)	(101)			(100)	(002)	(101)
AZ0	11	18	13	5	-2.92×10^{-2}	0.184	0.248	0.150
AZ1	15	19	17	10	-1.11×10^{-2}	0.182	0.255	0.147
AZ2	16	18	16	15	-3.15×10^{-4}	0.202	0.286	0.173
AZ3	17	11	9	4	8.27×10^{-2}	0.149	0.212	0.141

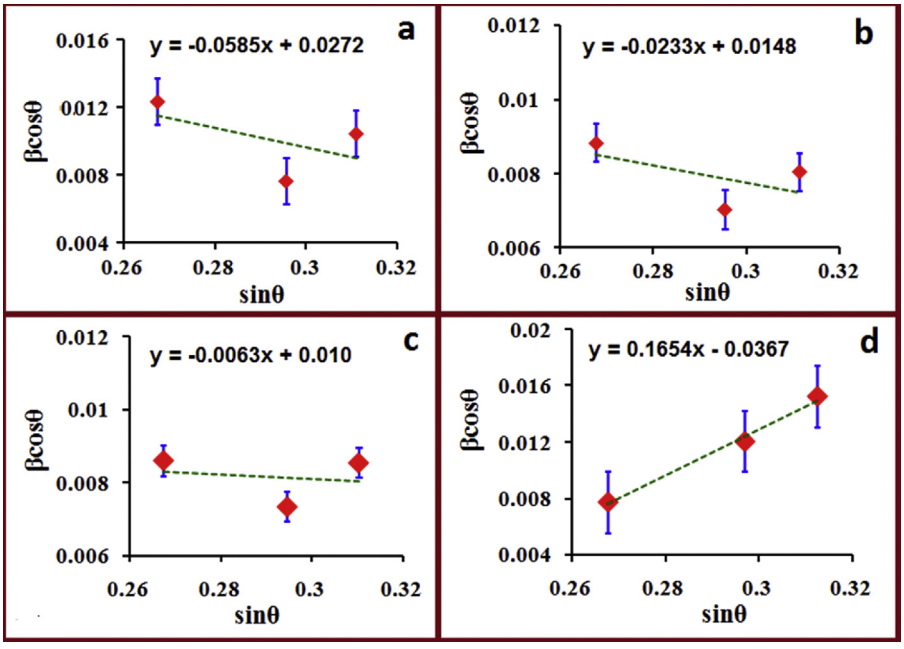

Fig. 3. Williamson-Hall plots for undoped and Al doped thin films. Here a–d correspond to samples AZ0, AZ1, AZ2 and AZ3, respectively.

obtained both by DS formula and WH plot. Here the a-lattice constant [33] is found to decrease for samples AZ1 and AZ3 but remains unchanged for sample AZ2. The c-lattice constant [33] increases for samples AZ1 and AZ2, and decreases for sample AZ3, maintaining the ratio c/a close to 1.56, Table 2. The anion-cation bond length lies in the range 2.007–2.013 Å. Dislocation density [38] representing the amount of defects in the film, calculated along each

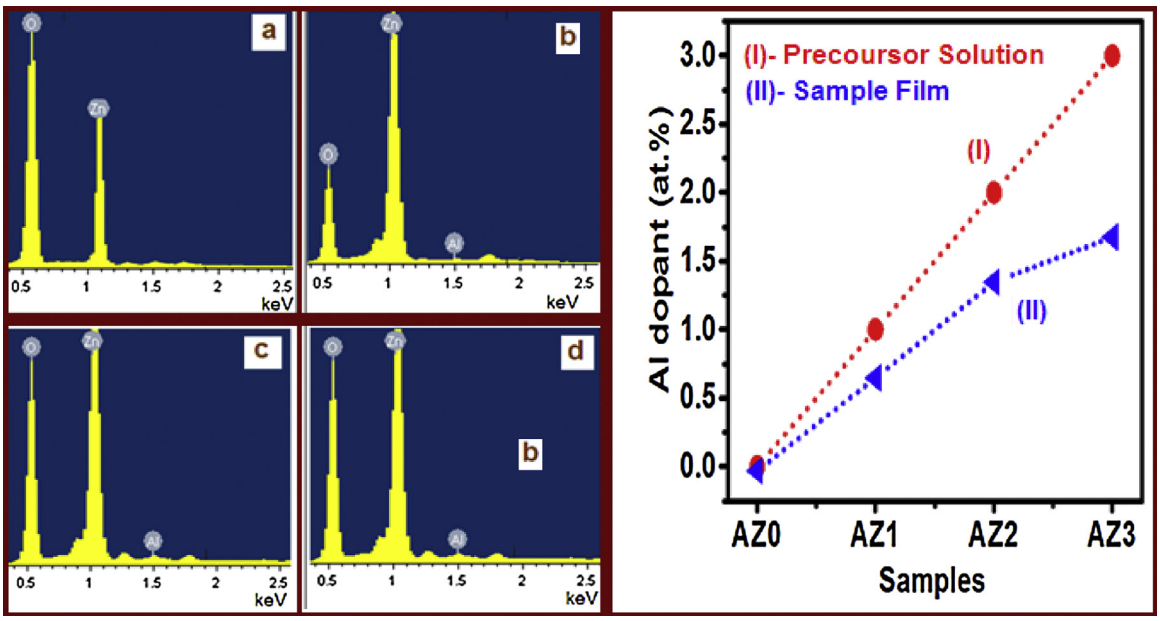

Fig. 4. EDX of undoped and Al doped films where a–d correspond to samples AZ0, AZ1, AZ2 and AZ3, respectively. Here curves (I) and (II) correspond to dopant amount in precursor solution and sample films, respectively.

Table 2
Lattice constant, bond length and dislocation density for undoped and Al doped films.

Samples	Lattice Constant		c/a	Anion-Cation Bond Length (Å)	Dislocation Density δ × (10^8 lines/mm^2)		
	a (Å)	c (Å)			(100)	(002)	(101)
AZ0	3.328	5.213	1.56	2.011	79.05	30.13	56.89
AZ1	3.326	5.218	1.56	2.011	40.60	25.77	33.64
AZ2	3.328	5.233	1.57	2.013	38.32	27.90	37.77
AZ3	3.324	5.189	1.56	2.007	31.04	75.60	120.69

plane using the formula $\delta = 1/t_{DS}^2$ [39] varies randomly from 10^9 to 10^{10} lines/mm^2 for the undoped and doped samples (Table 2).

The increase in c-lattice constant with increasing dopant amount up to 1.26 at.% indicates that the doping species Al^{3+} continues to lodge itself in the interstitials. A further increase in doping amount, 1.56 at.%, leads to shrinkage of the lattice constant suggesting a substitutional lodging of the Al dopant. Similar trend has been observed earlier in the case of Ca doped ZnO films [36] where the increased c-lattice constant started shrinking for much lower dopant concentration (0.88 at.%) as compared to that of Al. This may be attributed to the larger difference, nearly double, in the ionic radii of Ca^{2+} and Al^{3+}. Al^{3+}, being much smaller, is likely to lodge itself in interstitial space even for higher dopant amounts, beyond which substitution of Zn ions becomes inevitable. Even higher dopant amount may reduce crystallinity or lead to segregation of host and dopant.

3.2. EDX and SEM

The quantification of aluminium in the doped ZnO films is done by energy dispersive analysis. The EDX spectra (Fig. 4a–d) confirm the presence of Zn and O as the only species in the undoped sample AZ0. In the doped films, Al concentration is determined to be 0.62, 1.26 and 1.56 at.% whereas initially the respective precursor solutions were prepared with 1, 2 and 3 at.% Al doping. Here it should be mentioned that generally, in cases of wet chemical deposition methods, the actual concentration of dopant in the film is less than that in the precursor solution [33,40]. The concentration of Al in the precursor solutions as well as in the sample films has been shown through curves (I) and (II) of Fig. 4. The surface morphology of the four samples is shown in Fig. 5a–d. For undoped ZnO, i.e. sample AZ0, the surface is granular with grain size varying in the range 20–35 nm. For 0.62 at.% Al in ZnO (sample AZ1) the grains coalesce resulting in a flat smooth network over the surface. For sample AZ2 the network shrinks and separates out in smaller grains though not completely. As the concentration of Al increases further to 1.56 at.% (sample AZ3), clearly separated small cylindrical grains scattered over an almost smooth surface appear.

3.3. Optical transmission and band gap

The optical transmission spectra is recorded in the range of 300–900 nm for normal incidence using UV–vis-NIR spectrophotometer in the wavelength scanning mode, Fig. 6. As the amount of Al dopant is increased in the ZnO films the transmittance in the visible region increases monotonically from 60 to 80%. However, Chabane et al have reported a lowering in transmission by 10% on 8% Al doping [41]. The transmittance suddenly drops to ~10% near 372 nm for sample AZ0. This cut-off occurs for shorter and shorter wavelength as the amount of dopant is increased, leading to an enhancement in the band gap as well as in the width of transmission window. The absorption coefficient α and the optical band gap E_g are related by the formula $\alpha h\nu = (h\nu - E_g)^n$ where h is the Planck's constant and ν is the frequency of the incident radiation, n = 1/2 for 'direct' and 2 for 'indirect' band gap materials [42]. ZnO is a direct band gap material and so here n has been taken as 1/2 for band gap calculation. The absorption coefficient α is calculated from transmission data to obtain Tauc's plot from which the band gap E_g is determined (inset I of Fig. 6). The band gap for undoped and Al doped films, having thickness as 275, 227, 300 and

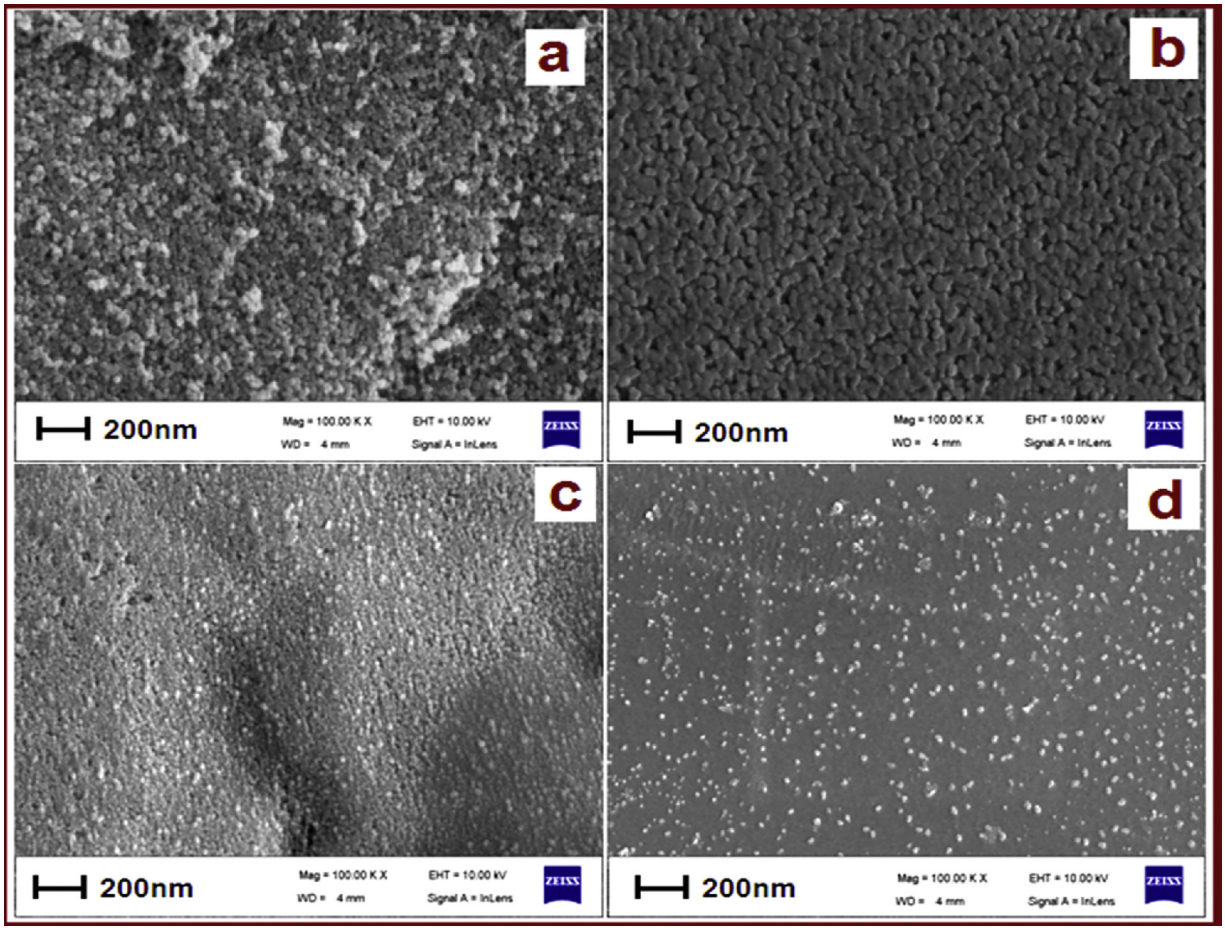

Fig. 5. SEM of undoped and Al doped films where a–d correspond to samples AZ0, AZ1, AZ2 and AZ3, respectively.

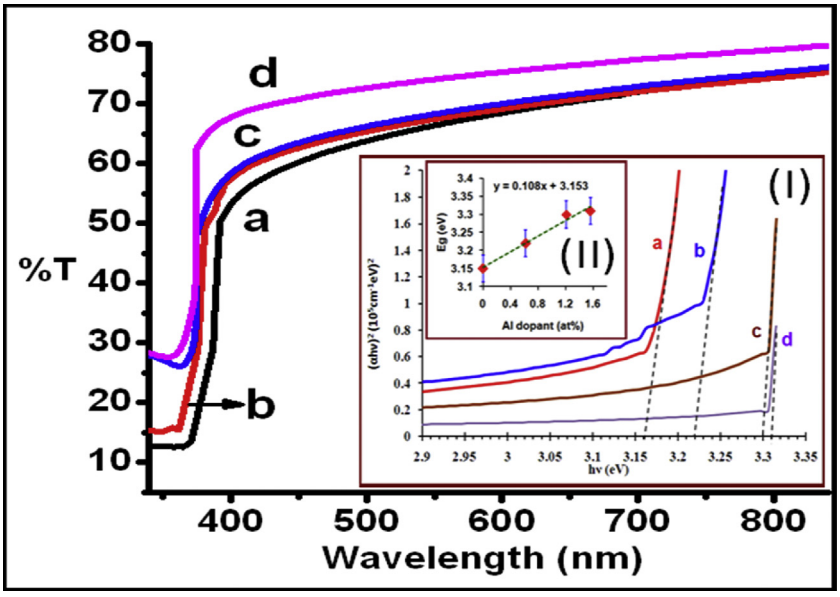

Fig. 6. Transmission spectra for undoped and Al doped thin films. Curves a–d correspond to samples AZ0, AZ1, AZ2 and AZ3 respectively. Insets (I) and (II) show Tauc's plot i.e. $(\alpha h\nu)^2$ vs. photon energy and variation in band gap with Al concentration along with the linear fit, respectively.

350 nm, is found to be 3.16(392 nm), 3.22(384 nm), 3.30(375 nm) and 3.31 eV (374 nm), respectively. Variation of the band gap with Al dopant concentration x (inset II of Fig. 6), follows the equation $E_g(x) = 0.108x + 3.153$. Thus, a band gap enhancement of 4.74% is obtained for a dopant concentration of 1.56 at.% Al in ZnO. This can be explained in terms of Burstein–Moss effect in case of donor dopants like aluminium. According to BM effect [43–45], increase of the carrier concentration results in a shift of the Fermi level and

blocking of some of the lowest states, thereby causing widening of the band gap resulting in the blue-shift of the absorption tail. Results from the literature on variation of band gap in Al doped ZnO are summarized in Table 3, to facilitate comparison.

In the present study the band gap widening of 0.06, 0.14 and 0.15 eV is obtained for 0.62, 1.26 and 1.56 at.% Al doping in ZnO films which compares favorably well with some results in literature as discussed here. Sharma et al. [19] have reported a band gap widening of 0.07, 0.08 and 0.05 eV for 1, 3 and 5 at.% Al doped ZnO films deposited by CVD. The band gap first increases up to 3 at.% doping and then drops but remains more than that for undoped one. This trend had been attributed to the stress in the films which varies in the corresponding manner. Park et al. [46] and Murali et al. [47] have reported an increment of 0.04 (3 wt.% doping) and 0.10 eV (10 wt.% doping), respectively which is much less than the present result even when the method of deposition used – magnetron sputtering- was highly sophisticated compared to spray pyrolysis used here. Lai et al. [48] have worked for 1 mol%Al doping and varying film thickness. For 271, 362 and 807 nm thickness the band gap widening have been reported to be 0.04, 0.07 and 0.08 eV which decreases with further increment in thickness, whereas in present study the films are much thinner, in the range of 275–350 nm, with nearly twice the band gap widening at 1.56 at.% doping. Wang et al. [49] reported a band gap widening of 0.02 and 0.04 eV for 1 and 2 at.% doping by sol gel method. Davoodi et al. [50] report E_g value of 3.23 and 3.24 eV for ZnO and AZO dip-coated thin films, respectively and have attributed the widening to the Burstein-Moss effect. Nakrela et al. [51] report a band gap increase from 3.20 to 3.27 eV on doping 4 at.%Al in ZnO thin films prepared by spray pyrolysis. However, contrasting results, i.e. reductions in band gap have also been reported. Optical band gap of 8%Al doped ZnO thin film reduces slightly from 3.29 to 3.27 eV for the films deposited on alkali free borosilicate glass and p-type silicon substrates using the Ultrasonic Spray Pyrolysis [41]. Rehman et al. [52] report a decrease in a band gap from 3.28 eV to 3.05 eV due to doping of 4 mol%Al in the films obtained by spray pyrolysis. Thermal annealing of Al doped ZnO thin films prepared by radio-frequency magnetron sputtering on quartz substrate has band gap reduction effect as it changes from 3.80 eV to 3.59 and 3.77 eV by annealing at 400 °C in N_2 and $N_2 + 4\%H_2$, respectively [53]. Electron irradiation [54] of doped film, 3 at.% aluminum dopant in ZnO, also led to a decrease in optical band gap from 2.72 to 2.46 eV as irradiation dose increased from 1 to 5 kGy. These thin films were deposited on glass substrates by spray pyrolysis technique.

There are two competing effects responsible for band gap shifts. One is Burstein-Moss effect and the other is band gap narrowing. The former occurs due to increasing carrier concentration and the movement of Fermi level in the conduction band whereas the latter occurs due to merger of the donor level and the conduction band above a critical carrier concentration termed as Mott density which is taken to be 4.5×10^{18} cm^3 [55,56]. Also, when the number of defects is high in ZnO based sample the defect states get more delocalized and may overlap with the valence band edge thereby raising it and leading to band gap reduction [57]. Transition metal dopants (Mn, Co in +2 state, Fe) also increase the band gap of ZnO which has been explained on the basis of exchange interaction of electrons in conduction and valence band with the d electrons of the dopants [58–60] and also in terms of sp hybridization [33,61].

In case of PLD, stochiometry is maintained and, therefore dopant concentration in the films remains same as that in the starting material. In both the Refs. [16,27] higher band gap enhancements as compared to present case are obtained but with a severe limitation of very small area deposition of PLD technique. The dopant amount was 4 and 3.3 at% in Refs. [28,45] and the methods used were CVD and magnetron sputtering, respectively. Compared to these cases, in the present study the dopant concentration is much less.

Table 3
Related results from literature for Al doped ZnO thin films including method of preparation, band gap, dopant amount and reference.

Sample/Substrate	Method of Preparation	Tuning of Band Gap	Change in Band Gap (eV)	Amount of Al Dopant	Explanation	Reference
Thin Film/Glass	PLD	3.27–3.57 eV (from graph)	+0.30	0–2 at.%	Burstein-Moss shift	Shukla et al. [16]
Thin Film/Sapphire (0006)	PLD	3.28–3.55 eV (from graph)	+0.27	0–2 at.%	Burstein-Moss shift	Das et al. [27]
Thin Film/soda-lime glass	CVD	3.28–3.59 eV	+0.31	0–4 at.%	Burstein-Moss shift	Lu et al. [28]
Thin Film/Quartz	CVD	3.19–3.27 eV	+0.08	0–3 at.%	Enhanced stress	Sharma et al. [19]
Thin Film/Si (001)	RF magnetron sputtering	3.20–3.41 eV	+0.21	0–3.3 at.%	Burstein-Moss shift	Kim et al. [45]
Thin Film/glass	DC Magnetron Sputtering	3.34–3.38 eV	+0.04	0–3 wt.%	Burstein-Moss shift	Park et al. [46]
Thin Film/soda-lime glass	Dc magnetron co-sputtering	3.29–3.39 eV	+0.10	1–10 wt.%	Burstein-Moss shift	Murali et al. [47]
Thin Film/glass	Spray pyrolysis	3.29–3.33 eV	+0.04	0–1 mol.%	Burstein-Moss shift	Lai et al. [48]
Thin Film/ glass	Sol-gel technique	3.26–3.30 eV	+0.04	0–2.0 at.%,	Burstein-Moss shift	Wang et al. [49]
Thin Film/glass	Dip-coating	3.23 and 3.24 eV,	+0.01	1 at.%	Burstein-Moss shift	Davoodi et al. [50]
Thin Film/glass	spray pyrolysis	3.20–3.27 eV	+0.07	4 at.%Al	–	Nakrela et al. [51]
Thin Film/glass	Spray pyrolysis	3.16–3.31 eV	+0.15	0–1.56 at. %	Burstein-Moss shift	*Present study*
Thin Film/glass	Spray pyrolysis	3.28–3.05 eV	–0.23	0–4 mol.%	–	Rahman et al. [52]
Thin Film/borosilicate glass and p-type silicon substrates	Ultrasonic Spray Pyrolysis	3.29–3.27 eV	–0.02	8%Al doped	–	Chabane et al. [41]

In all the above reports except films prepared by PLD, the maximum band gap enhancement obtained is approximately 1.2% which is much less compared to that presently reported. An enhancement of 4.74% in the band gap by quite small increment in dopant concentration (0–1.56 at.%) makes the present films, which are prepared by spray pyrolysis, much attractive for the fabrication of light emitting devices with a much sought-for benefit of large area fabrication.

3.4. Photoluminescence

As mentioned earlier the excitation wavelength is taken to be 325 nm (3.81 eV) [27], an energy much larger than the band gaps obtained in Section 3.3. PL emission spectra of all the samples show one peak in UV region and three peaks in the visible region of spectrum, Fig. 7. UV emission is of much higher intensity than those of the other peaks. For all the samples UV emission peak occurs at ~389 nm (3.18 eV) whereas the band gaps for these samples are of 3.16, 3.22, 3.30 and 3.31 eV, respectively and as seen in previous section. Therefore, for undoped ZnO, UV emission appears to be a band to band transition as the emitted energy is more than the band-gap whereas for the three doped-ZnO samples the UV emission peaks are Stokes shifted with respect to the absorption edge in all the films indicating near band edge (NBE) or excitonic transitions. The PL emission near to its band gap is assigned as NBE emission and that occurring in visible region, in the case of ZnO, is assigned as defect related emission. It has also been reported by many authors. It may be recalled that if the energy of fluorescence emission is lesser than that of excitation, the emission is known as Stokes shifted. Occurrence of Stokes shift is important for practical applications as it facilitates separation of strong excitation light from weak fluorescence using appropriate optics. The three peaks in the visible region occur at 446, 460 and 485 nm and are defect related. Occurrence of UV emission from all the samples reflects upon the good crystalline quality of the present films grown by spray pyrolysis. The intensity of the UV emission is found to depend on the amount of Al doping and increases monotonically with increase in dopant amount. More importantly, defect emissions are suppressed remarkably as Al concentration increases i.e. for samples AZ2 and AZ3 (Fig. 7 inset (A)) which is explained later. The ratio of intensities of UV to visible emission (at wavelength 486 nm), I_{uv}/I_{vis}, increases from 5.03 to 10.26 as the dopant increases from 0 to 1.56 at% via a low of 2.77 at 0.62 at.%. (Fig. 7 inset (B)). As mentioned earlier, the energy of UV emission remains the same for varying dopant-amounts in the present films. Similar observation has been reported by Park et al. [46], Sharma et al. [62], Das et al. [63] and Das et al. [27] where Al doped ZnO films are deposited by DC magnetron sputtering, chemical vapor deposition, sol-gel dip coating and sequential pulsed laser deposition respectively. In Ref. [46] UV emission is at 3.43 eV energy of which does not depend on Al concentration although emission intensity increases monotonically. In Ref. [62] UV emission is at 380 nm which changes to 377 nm as dopant concentration increases from 0 to 3 at% whereas emission intensity remains almost the same as inferred from the reported PL plot. Exactly same shift in UV emission has been reported by Das et al. [63] but for 1 at.%Al doped sample. In Ref. [27] where PLD is used, UV emission occurs at ~370 nm which shows blue-shift with increase in dopant concentration from 0 to 5 at.% and the emission intensity decreases markedly in a monotonous manner which is reported to be due to deterioration in the crystalline quality of the films on increased Al doping. It appears that films obtained using PLD, being a quite sophisticated method, are more sensitive to doping. In Refs. [35,44]discussed above, as well as in the present study, UV emission intensity either remains unaltered or increases with increase in aluminium dopant concentration but the defect related emissions or deep-level emissions get suppressed in all the four cases [Refs. [18,35,44] and the present study].

In literature deep-level emission has been attributed to the native defects like oxygen vacancies (V_o), zinc vacancies (V_{Zn}), interstitial zinc (Zn_i) sites [46] and antisites [64–66]. Coexistence of V_{Zn} with Zn_i is highly probable as also shown by Lin et al. [67]. References [67,68] have shown the intrinsic defect levels of ZnO films (of band gap 3.36 eV) using full-potential linear muffin-tin orbital

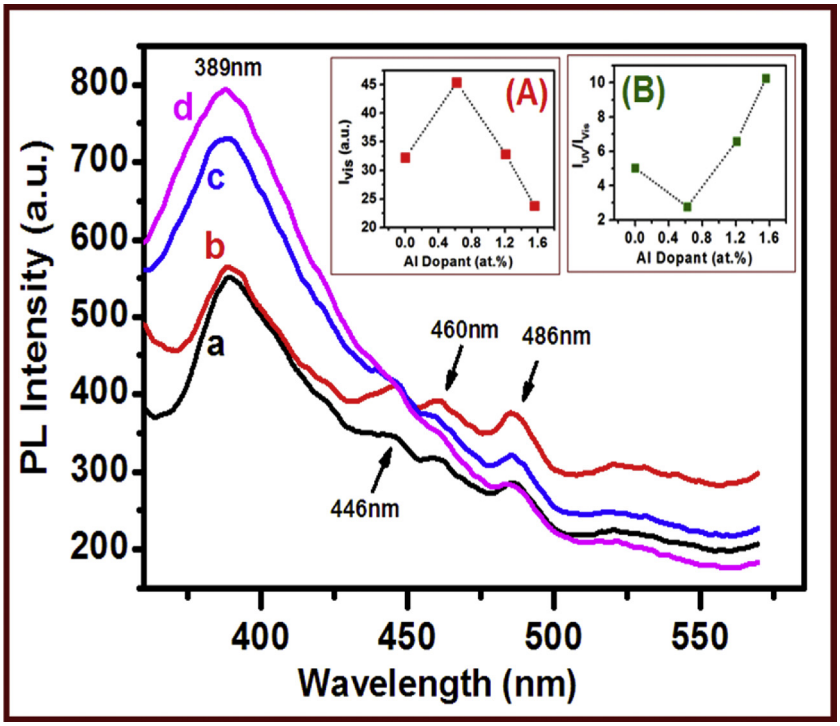

Fig. 7. Photoluminescence spectra of undoped and Al doped thin films. Curves a–d correspond to samples AZ0, AZ1, AZ2 and AZ3, respectively. The insets A and B show variation in intensity of emission I_{vis} at wavelength 486 nm and the ratio I_{UV}/I_{vis} with Al concentration, respectively.

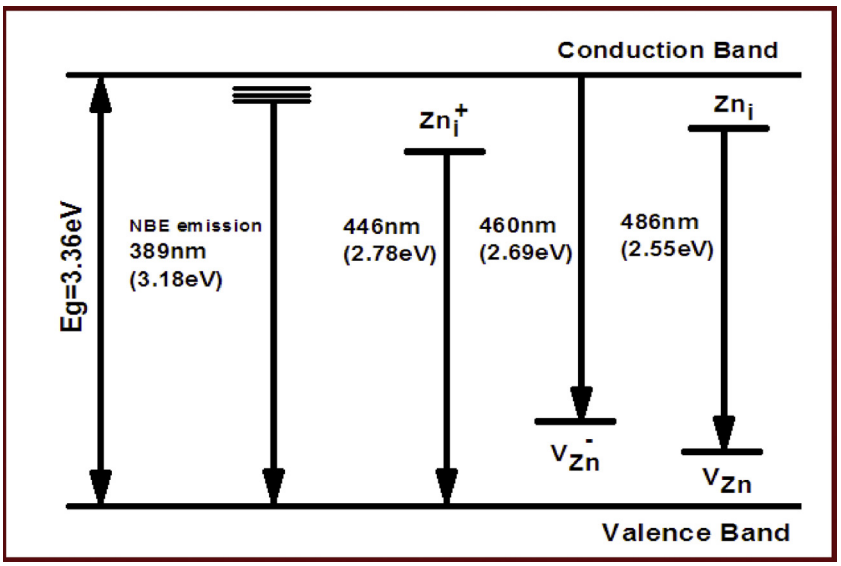

Fig. 8. Schematic band diagram of defect levels based on photoluminescence data.

method. Zn_i levels are at 2.90 eV, Zn_i^+ levels are at 2.75 eV and V_{Zn} are at 0.30 eV above the valance band. V_o, O_i and O_{Zn} are at 1.62, 2.28 and 3.28 eV below the conduction band. V_{Zn}^- is at ~2.69 eV below the conduction band. These energy levels are shown in Fig. 8 and accordingly the blue green luminescence at 486 nm (2.55 eV) occurring in our experiment can be correlated to the electronic transition from the donor energy level of Zn_i to the acceptor level of V_{Zn}; the blue emission at 460 nm (2.69 eV) corresponds to conduction band – V_{Zn}^- transition and the violet emission at 446 nm(2.78 eV) corresponds to Zn_i^+ to valence band transition. The presence of Al promotes oxygen diffusion in ZnO matrix which leads to the suppression of oxygen vacancies related defects [69,70]. Presence of Al^{3+} also reduces the concentration of $Zn^{2+}{}_i$ to maintain charge neutrality. Besides, method of deposition also plays a role in deciding the equilibrium of various types of defects and optical and crystalline quality of films. Thus, appropriate amount of Al doping in ZnO can be used to enhance the intensity and quality of UV emission as rising concentration of Al dopant in spray deposited ZnO films suppresses defect emission. The presence of Al interstitials indicated by the increase of lattice constant, in addition to Zn increases the number of donor levels thereby increasing the defect emission from sample AZ1 as compared to that from AZ0. Similarly in sample AZ2 also, having increased dopant amount, the number of donor levels have increased. In spite of this fact, the defect emission decreases. Such an effect owes to competing phenomenon of quenching of the defect fluorescence with increase of Al concentration as they interfere with each other's sphere of activity. In Ref. [36] quenching set in when the Ca started substitution of Zn which was indicated by shrinkage of lattice constant. Here in case of Al, the ionic radii is much smaller and therefore more and more Al^{3+} can accommodate themselves in interstitial and result in elongated lattice constant. Substitution of Zn predominates at comparatively higher concentrations. Since more and more Al^{3+} ions are located in closed vicinity, quenching sets in leading to diminished defect emission in spite of large number of donor levels.

On the contrary in earlier investigations the UV emission, which is an NBE emission, showed blue shift with increase in dopant concentration for the sol-gel spin coated films. For Ca doped ZnO, this peak shifted from 399 to 392 nm as dopant concentration increased from 0 to 1.47 at% leading to a tuning of UV emission by 0.055 eV [36]. For Sr doped ZnO, this peak shifted from 399 to 393 nm as dopant concentration increased from 0 to 3 at% leading to a tuning of UV emission by 0.053 eV [71]. For Fe doped ZnO, this peak shifted from 398 to388 nm as dopant concentration increased from 0 to 3 at% leading to a tuning of UV emission by 0.076 eV [33].

4. Conclusions

Hexagonal wurtzite aluminium doped zinc oxide nanocrystalline films with crystallite size less than 19 nm are obtained on glass substrate using spray pyrolysis, with preferred orientation along (002) plane. The films are optically transparent with transmission around 75%. With increasing dopant concentration from 0 to 1.56 at.% the band gap increases monotonically from 3.16 to 3.31 eV facilitating a band gap tuning of 4.74% and a continuously increasing width of the transmission window. Ultraviolet photoluminescence at 389 nm of continuously increasing intensity with increase in dopant is obtained which reflects on good crystalline quality of the films. More importantly, dopant Al suppresses the defect emissions remarkably with its increasing concentration in ZnO. The surface is granular with grain size varying in the range 20–35 nm. Small cylindrical grains with reduced areal density appear over an almost smooth surface as the amount of dopant increases to 1.56 at%. The band gap enhancement obtained here is much larger as compared to those reported in literature which are at the most ~1.2%, excluding the films prepared by PLD. The band gap tuning by quite small increment in dopant concentration makes the present films, much attractive for the fabrication of light emitting devices with a much sought-for benefit of large area fabrication.

Acknowledgement

Award of Research Assistantship to one of the authors, Nishant Kumar from CSTUP India vide project no.CST/D-1129. Authors are also thankful to DST New Delhi India for providing UV–vis-NIR spectrometer facility (vide project no.SR/S2/CMP–0028/2010) and UGC through SAP for providing Fluorescence spectrometer facility.

References

[1] H. Kim, C.M. Gilmore, A. Pique, J.S. Horwitz, H. Murata, Z.H. Kafafi, D.B. Chrisey, Electrical optical, and structural properties of indium-tin-oxide thin films for organic light-emitting devices, J. Appl. Phys. 86 (1999) 6451–6461.

[2] H. Kim, C.M. Gilmore, J.S. Horwitz, A. Pique, H. Murata, G.P. Kushto, R. Schlaf, Z.H. Kafafi, D.B. Chrisey, Transparent conducting aluminum-doped zinc oxide thin films for organic light-emitting devices, Appl. Phys. Lett. 76 (2000) 259.
[3] H. Kim, A. Pique, J.S. Horwitz, H. Murata, Z.H. Kafafi, C.M. Gilmore, D.B. Chrisey, Effect of aluminum doping on zinc oxide thin films grown by pulsed laser deposition for organic light-emitting devices, Thin Solid Films 377–378 (2000) 798–802.
[4] J.-L. Zhao, X.-M. Li, J.-M. Bian, W.-D. Yu, X.-D. Gao, Structural, optical and electrical properties of ZnO films grown by pulsed laser deposition (PLD), J. Cryst. Growth 276 (2005) 507–512.
[5] R. Das, S. Ray, Thickness dependence of the properties of magnetron sputtered ZnO: Al films and its application in a-Si:H thin film solar cell, Indian J. Phys. 78 (2004) 901–906.
[6] Y. He, J. Kanicki, High-efficiency organic polymer light-emitting heterostructure devices on flexible plastic substrates, Appl. Phys. Lett. 76 (2000) 661–663.
[7] S.-H. Lee, Se-H. Han, H.S. Jung, H. Shin, J. Lee, J.-H. Noh, S. Lee, I.-S. Cho, J.-K. Lee, J. Kim, H. Shin, Al-doped ZnO thin film: a new transparent conducting layer for ZnO nanowire-based dye-sensitized solar cells, J. Phys. Chem. C 114 (2010) 7185–7189.
[8] S. Kaps, S. Bhowmick, J. Grottrup, V. Hrkac, D. Stauffer, H. Guo, O.L. Warren, J. Adam, L. Kienle, A.M. Minor, R. Adelung, Y.K. Mishra, Piezoresistive response of quasi-one-dimensional ZnO nanowires using an in situ electromechanical device, ACS Omega 2 (2017) 2985–2993.
[9] V. Postica, J. Gröttrup, R. Adelung, O. Lupan, A.k. kMishra, N.H.d. Leeuw, N. Ababii, J.F.C. Carreira, J. Rodrigues, N.B. Sedrine, M.R. Correia, T. Monteiro, V. Sontea, Y.K. Mishra, Multifunctional materials: a case study of the effects of metal doping on ZnO tetrapods with bismuth and tin oxides, Adv. Funct. Mater. 27 (2017) 1604676.
[10] I. Tiginyanu, L. Ghimpu, J. Gröttrup, V. Postolache, M. Mecklenburg, M.A. Stevens-Kalceff, V. Ursaki, N. Payami, R. Feidenhansl, Karl Schulte, R. Adelung, Y.K. Mishra, Strong light scattering and broadband (UV to IR) photoabsorption in stretchable 3D hybrid architectures based on aerographite decorated by ZnO nanocrystallites, Sci. Rep. 6 (32913) (2016) 1–11.
[11] C. Klingshirn, ZnO: From basics towards applications, Phys. Status Solidi B 244 (2007) 3027–3073.
[12] X. Jin, M. Götz, S. Wille, Y.K. Mishra, R. Adelung, C. Zollfrank, A novel concept for self-reporting materials: stress sensitive photoluminescence in ZnO tetrapod filled elastomers, Adv. Mater. 25 (2013) 1342–1347.
[13] K.J. Saji, K. Tian, M. Snure, A. Tiwari, 2D tin monoxide—an unexplored p-type van der waals semiconductor: material characteristics and field effect transistors, Adv. Electron. Mater. 2 (2016) 1500453.
[14] Y.K. Mishra, S. Kaps, A. Schuchardt, I. Paulowicz, X. Jin, D. Gedamu, S. Freitag, M. Claus, S. Wille, A. Kovalev, S.N. Gorb, R. Adelung, Fabrication of macroscopically flexible and highly porous 3D semiconductor networks from interpenetrating nanostructures by a simple flame transport approach part, Part. Syst. Charact. 30 (2013) 775–783.
[15] T. Reimer, I. Paulowicz, R. Röder, S. Kaps, O. Lupan, S. Chemnitz, W. Benecke, C. Ronning, R. Adelung, Y.K. Mishra, Single step integration of ZnO Nano- and microneedles in Si trenches by novel flame transport approach: whispering gallery modes and photocatalytic properties, ACS Appl. Mater. Interfaces 6 (2014) 7806–7815.
[16] R.K. Shukla, A. Srivastava, A. Srivastava, K.C. Dubey, Growth of transparent conducting nanocrystalline Al doped ZnO thin films by pulsed laser deposition, J. Cryst. Growth 294 (2006) 427–431.
[17] A. Sarkar, S. Ghosh, S. Chaudhuri, A.K. Pal, Studies on electron transport properties and the burstein-moss shift in indium-doped ZnO films, Thin Solid Films 204 (1991) 255–264.
[18] V. Bhosle, A. Tiwari, J. Narayan, Electrical properties of transparent and conducting Ga doped ZnO, J. Appl. Phys. 100 (2006) 033713.
[19] B.K. Sharma, N. Khare, Stress-dependent band gap shift and quenching of defects in Al-doped ZnO films, J. Phys. D: Appl. Phys. 43 (2010) 465402.
[20] J.H. Lee, B.O. Park, Transparent conducting ZnO:Al, In and Sn thin films deposited by the sol-gel method, Thin Solid Films 426 (2003) 94–99.
[21] M. Ohyama, H. Kozuka, T. Yoko, Sol-gel preparation of transparent and conductive aluminum-doped zinc oxide films with highly preferential crystal orientation, J. Am. Ceram. Soc. 81 (1998) 1622–1632.
[22] Y. Yamamoto, K. Saito, K. Takakashi, M. Konagai, Preparation of boron-doped ZnO thin films by photo-atomic layer deposition, Sol. Energy Mater. Sol. Cells 65 (2001) 125–132.
[23] A. Sanchez-Juarez, A. Tiburcio-Silver, A. Oritz, E.P. Zironi, J. Rickards, Electrical and optical properties of fluorine-doped ZnO thin Films prepared by spray pyrolysis, Thin Solid Films 333 (1998) 196–202.
[24] Y. Natsume, H. Sakata, Electrical and optical properties of zinc oxide films post-annealed in H_2 after fabrication by sol-gel process, Mater. Chem. Phys. 78 (2002) 170–176.
[25] Z. Zhan, J. Zhang, Q. Zheng, D. Pan, J. Huang, F. Huang, Z. Lin, Strategy for preparing Al-doped ZnO thin film with high mobility and high stability, Cryst. Growth Des. 11 (2011) 21–25.
[26] D. Mishra, A. Srivastava, A. Srivastava, R.K. Shukla, Bead structured nanocrystalline ZnO thin films: synthesis and LPG sensing properties, Appl. Surf. Sci. 255 (2008) 2947–2950.
[27] A.K. Das, P. Misra, A. Bose, S.C. Joshi, R. Kumar, T.K. Sharma, L.M. Kukreja, Structural, electrical and optical characteristics of Al doped ZnO films grown by sequential pulsed laser deposition, Phys. Express 3 (2013) 15.
[28] J.G. Lu, S. Fujita, T. Kawaharamura, H. Nishinaka, Y. Kamada, T. Ohshima, Z.Z. Ye, Y.J. Zeng, Y.Z. Zhang, L.P. Zhu, H.P. He, B.H. Zhao, Carrier concentration dependence of band gap shift in n—type ZnO:Al films, J. Appl. Phys. 101 (2007) 083705.
[29] K.P. Misra, R.K. Shukla, A. Srivastava, A. Srivastava, Blueshift in optical band gap in nanocrystalline $Zn_{1-x}Ca_xO$ films deposited by sol-gel method, Appl. Phys. Lett. 95 (2009) 031901.
[30] A.K. Das, P. Misra, L.M. Kukreja, Effect of Si doping on electrical and optical properties of ZnO thin films grown by sequential pulsed laser deposition, J. Phys. D: Appl. Phys. 42 (2009) 165405.
[31] H.K. Yadav, V. Gupta, A comparative study of ultraviolet photoconductivity relaxation in zinc oxide (ZnO) thin films deposited by different techniques, J. Appl. Phys. 111 (2012) 102809.
[32] K.-Y. Wu, C.-C. Wang, D.-H. Chen, Preparation and conductivity enhancement of Al-doped zinc oxide thin films containing trace Ag nanoparticles by the sol-gel process, Nanotechnology 18 (2007) 305604.
[33] A. Srivastava, N. Kumar, S. Khare, Enhancement in UV emission and band gap by Fe doping in ZnO thin films, Opto-Electron. Rev. 22 (2014) 68–76.
[34] Y.W. Li, J.L. Sun, X.J. Meng, J.H. Chu, W.F. Zhang, Structural and optical properties of $Ba(Co_x, Ti_{1-x})O_3$ thin films fabricated by sol-gel process, Appl. Phys. Lett. 85 (2004) 1964–1966.
[35] F.W. Jones, The measurement of particle size by the X-ray method, Proc. R. Soc. London 66 (1938) 16–43.
[36] A. Srivastava, N. Kumar, K.P. Misra, S. Khare, Blue-light luminescence enhancement and increased band gap from calcium-doped zinc oxide nanoparticle films, Mater. Sci. Semicond. Process. 26 (2014) 259–266.
[37] G.K. Williamson, W.H. Hall, X-ray line broadening from filed aluminium and wolfram, Acta Metall. 1 (1953) 22–31.
[38] S. Kahraman, F. Bayansal, H.M. Çakmak, H.A. Çetinkara, H.S. Güder, Synthesis and characterization of undoped and tin-doped ZnO nanostructures, Appl. Phys. A 109 (2012) 87–93.
[39] N. Kumar, A. Srivastava, Faster photoresponse, enhanced photosensitivity and photoluminescence in nanocrystalline ZnO films suitably doped by Cd, J. Alloys Compd. 706 (2017) 438–446.
[40] A. Douayar, P. Prieto, G. Schmerber, K. Nouneh, R. Diaz, I. Chaki, S. Colis, A. El Fakir, N. Hassanain, A. Belayachi, Z. Sekkat, A. Slaoui, A. Dinia, M. Abd-Lefdi, Investigation of the structural, optical and electrical properties of Nd-doped ZnO thin films deposited by spray pyrolysis, Eur. Phys. J. Appl. Phys. 61 (2013) 0304.
[41] L. Chabane, N. Zebbar, M. Kechouane, M.S. Aida, M. Trari, Al-doped and in-doped ZnO thin films in heterojunctions with silicon, Thin Solid Films 605 (2016) 57–63.
[42] A. Srivastava, K.P. Misra, Band gap control and photoluminescence properties of $Ba(Co_{2x}Ti_{1-x})O_3$ thin films prepared by sol-gel method, Appl. Phys. A 117 (2014) 917–926.
[43] E. Burstein, Anomalous optical absorption limit in InSb, Phys. Rev. 93 (1954) 632–633.
[44] T.S. Moss, The interpretation of the properties of indium antimonide, Proc. Phys. Soc. London Ser. B 67 (1954) 775.
[45] Y. Kim, W. Lee, D.-R. Jung, J. Kim, S. Nam, H. Kim, B. Park, Optical and electronic properties of post-annealed ZnO:Al thin films, Appl. Phys. Lett. 96 (2010) 171902.
[46] S.H. Park, S.E. Park, J.C. Lee, P.K. Song, Photoluminescence characterization of Al-doped ZnO films deposited by using DC magnetron sputtering, J. Korean Phys. Soc. 54 (2009) 1344–1347.
[47] B. Murali, J. Parui, M. Madhuri, S.B. Krupanidhi, An insight to the low temperature conduction mechanism of c-axis grown Al-doped ZnO, a widely used transparent conducting oxide, J. Phys. D: Appl. Phys. 48 (2015) 015301.
[48] H. Hung-Chun Lai, T. Basheer, V.L. Kuznetsov, R.G. Egdell, R.M.J. Jacobs, M. Pepper, P.P. Edwards, Dopant-induced bandgap shift in Al-doped ZnO thin films prepared by spray pyrolysis, J. Appl. Phys. 112 (2012) 083708.
[49] M. Wang, K.E. Lee, S.H. Hahn, E.J. Kim, S. Kim, J.S. Chung, E.W. Shin, C. Park, Optical and photoluminescent properties of sol-gel Al-doped ZnO thin films, Mater. Lett. 61 (2007) 1118.
[50] A. Davoodi, M. Tajally, O. Mirzaee, A. Eshaghi, Fabrication and characterization of optical and electrical properties of Al-Ti Co-doped ZnO nano-structured thin film, J. Alloys Compd. 657 (2016) 296–301.
[51] A. Nakrela, N. Benramdane, A. Bouzidi, Z. Kebba, M. Medles, C. Mathieu, Site location of Al-dopant in ZnO lattice by exploiting the structural and optical characterisation of ZnO:Al thin films, Results Phys. 6 (2016) 133–138.
[52] M.M. Rahman, M.K.R. Khan, M.R. Islam, M.A. Halim, M. Shahjahan, M.A. Hakim, D.K. Saha, J. Uddin Khan, Effect of Al doping on structural electrical, optical and photoluminescence properties of nano-structural ZnO thin films, J. Mater. Sci. Technol. 28 (2012) 329.
[53] W. Yang, Z. Wu, Z. Liu, A. Pang, Y.-L. Tu, Z.C. Feng, Room temperature deposition of Al-doped ZnO films on quartz substrates by radio-frequency magnetron sputtering and effects of thermal annealing, Thin Solid Films 519 (2010) 31–36.
[54] A. Antony, S. Pramodini, P. Poornesh, I.V. Kityk, A.O. Fedorchuk, G. Sanjeev, Influence of electron beam irradiation on nonlinear optical properties of Al doped ZnO thin films for optoelectronic device applications in the cw laser regime, Opt. Mater. 62 (2016) 64–71.
[55] J. Kumar, A.K. Srivastava, Band gap narrowing in zinc oxide-based semiconductor thin films, J. Appl. Phys. 115 (2014) 134904.

[56] K.G. Saw, N.M. Aznan, F.K. Yam, S.S. Ng, S.Y. Pung, New insights on the burstein-moss shift and band gap narrowing in indium-doped zinc oxide thin films, PLoS One 10 (2015) 1–17.
[57] J. Wang, Z. Wang, B. Huang, Y. Ma, Y. Liu, X. Qin, X. Zhang, Y. Dai, Oxygen vacancy induced band-gap narrowing and enhanced visible light photocatalytic activity of ZnO, ACS appl, Mater. Interfaces 4 (2012) 4024–4030.
[58] R.B. Bylsma, M. Becker, J. Kossut, U. Debska, Dependence of energy gap on x and T in $Zn_{1-x}Mn_x$ Se: the role of exchange interaction, Phys. Rev. B 33 (1986) 8207.
[59] J. Diouri, J.P. Lascaray, M. El Amrani, Effect of the magnetic order on the optical-absorption edge in $Cd_{1-x}Mn_xTe$, Phys. Rev. B 31 (1985) 7995–7999.
[60] T. Fukumura, Z. Jin, A. Ohtomo, H. Koinuma, M. Kawasaki, An oxide-diluted magnetic semiconductor: Mn-doped ZnO, Appl. Phys. Lett. 75 (1999) 3366–3368.
[61] J.K. Furdyna, Diluted magnetic semiconductors, J. Appl. Phys. 64 (1988) R29.
[62] B.K. Sharma, N.j Khare, D. Haranath, Photoluminescence lifetime of Al-doped ZnO films in visible region, Solid State Commun. 150 (2010) 2341–2345.
[63] A. Das, P.G. Roy, A. Dutta, S. Sen, P. Pramanik, D. Das, A. Banerjee, A. Bhattacharyya, Mg and Al co-doping of ZnO thin films: effect on ultraviolet photoconductivity, Mater. Sci. Semicond. Process. 54 (2016) 36–41.
[64] F. Wen, W. Li, J.-H. Moon, J.H. Kim, Hydrothermal synthesis of ZnO:Zn with green emission at low temperature with reduction process, Solid State Commun. 135 (2005) 34–37.
[65] K. Vanheusden, W.L. Warren, C.H. Seager, D.R. Tallant, J.A. Voight, Mechanisms behind green photoluminescence in ZnO phosphor powders, J. Appl. Phys. 79 (1996) 7983.
[66] Y.L. Shi, J. Wang, H.L. Li, Photoluminescence behavior of purpose-built ZnO arrays on different growth substrates, Appl. Phys. A 79 (2004) 1797–1799.
[67] B. Lin, Z. Fu, Y. Jia, Green luminescent center in undoped zinc oxide films deposited on silicon substrates, Appl. Phys. Lett 79 (2001) 943.
[68] P.S. Xu, Y.M. Sun, C.S. Shi, F.Q. Xu, H.B. Pan, Nucl. Instrum. Methods Phys. Res. B 199 (2003) 286.
[69] H. Ryoken, I. Sakaguchi, N. Ohashi, T. Sekiguchi, S. Hishita, H. Haneda, Non-equilibrium defects in aluminum-doped zinc oxide thin films grown with a pulsed laser deposition method, J. Mater.Res. 20 (2005) 2866–2872.
[70] Y. Liu, H. Zhang, X. An, C. Gao, Z. Zhang, J. Zhou, M. Zhou, E. Xie, Effect of Al doping on the visible photoluminescence of ZnO nanofibers, J. Alloy. Compd. 506 (2010) 772–776.
[71] A. Srivastava, N. Kumar, K.P. Misra, S. Khare, Enhancement of band gap of ZnO nanocrystalline films at a faster rate using Sr dopant, Electron. Mater. Lett. 10 (2014) 703–711.